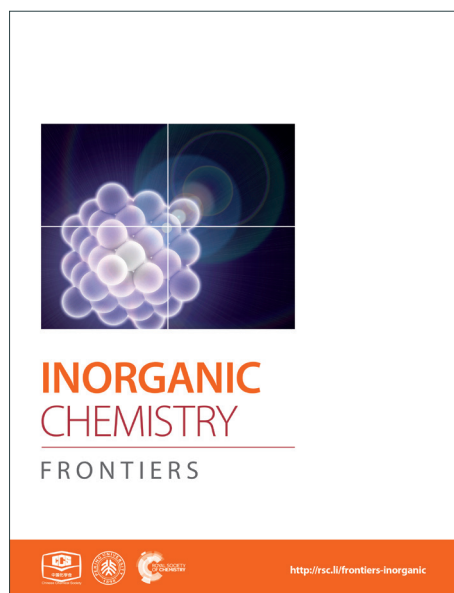
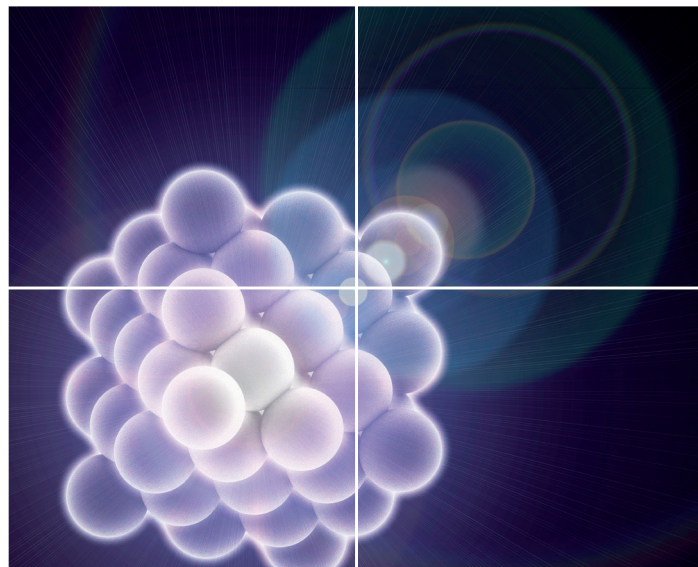


# INORGANIC CHEMISTRY

FRONTIERS

Accepted Manuscript



This is an *Accepted Manuscript*, which has been through the Royal Society of Chemistry peer review process and has been accepted for publication.

*Accepted Manuscripts* are published online shortly after acceptance, before technical editing, formatting and proof reading. Using this free service, authors can make their results available to the community, in citable form, before we publish the edited article. We will replace this *Accepted Manuscript* with the edited and formatted *Advance Article* as soon as it is available.

You can find more information about *Accepted Manuscripts* in the [Information for Authors](#).

Please note that technical editing may introduce minor changes to the text and/or graphics, which may alter content. The journal's standard [Terms & Conditions](#) and the [Ethical guidelines](#) still apply. In no event shall the Royal Society of Chemistry be held responsible for any errors or omissions in this *Accepted Manuscript* or any consequences arising from the use of any information it contains.

Cite this: DOI: 10.1039/c0xx00000x

www.rsc.org/xxxxxx

ARTICLE TYPE

# Hetero-nuclear Coordinated Compounds for Use in High-Performance Supercapacitor Electrode Materials Design

Liwei Mi,<sup>\*a</sup> Yang Gao,<sup>a,b</sup> Shizhong Cui,<sup>a</sup> Hongwei Hou<sup>b</sup> and Weihua Chen<sup>\*b</sup>

Received (in XXX, XXX) Xth XXXXXXXXXX 20XX, Accepted Xth XXXXXXXXXX 20XX

DOI: 10.1039/b000000x

**Abstract:** Single crystals of cobalt coordination compound were obtained by one-pot hydrothermal reaction. Nickel ion exchange was used to produce Ni–Co hetero-metal compound with tunable chemical composition. Using nickel-exchanged compound as the precursor, we developed a simple chemical reaction to synthesize large-scale 3D hierarchical  $\text{Ni}_x\text{Co}_{3-x}\text{S}_4$  ( $x = 0.15\text{--}0.42$ ) microflowers under ambient conditions. As an electrode material for supercapacitors, the discharge capacitance of  $\text{Ni}_{0.42}\text{Co}_{2.58}\text{S}_4$  microflowers is approximately one and a half times higher than the discharge capacitance value of  $\text{Ni}_{0.15}\text{Co}_{2.75}\text{S}_4$  at a current density of  $0.5 \text{ A g}^{-1}$ .

## Introduction

Single crystals are an essential part of nature and have been the focus of recent research activities because of their distinct physical characteristics; such characteristics are related to polycrystal properties, such as thermal conductivity<sup>1a</sup> and electron transport properties.<sup>1b, c, d</sup> Compared with a single crystal diamond, a polycrystalline diamond exhibits poor thermal conductivity.<sup>1</sup> Silicon-based materials also have excellent electron transport properties; single crystal silicon has been widely used in solar energy conversion<sup>1b, c</sup> and data storage.<sup>1d</sup> Therefore, using a single crystal as a template to obtain another new single crystal may be an efficient and simple option to achieve the state of coexisting properties of multi-metal coordination complexes.

In single-crystal to single-crystal (SCSC) transformation, original lattice parameters are left unchanged or are minimally changed in the single crystal during phase transition.<sup>2, 3, 4</sup> Various approaches, such as those involving light, heat, and pressure have been proposed to achieve SCSC transformation in coordination chemistry.<sup>3</sup> Our previous studies focused on cation exchange-induced tunable properties of the nanoporous octanuclear Cu(II) wheel,<sup>2a</sup> polymeric cadmium ferrocene-1,1-disulfonates,<sup>5a</sup> and ferrocenyl-based inclusion complexes.<sup>5b</sup> We believe that the central metal ion exchange can serve as a powerful method to modify properties of crystalline materials by varying the central metal ions. Under this process, we can control the main performance of crystalline materials by adjusting the ratio of central metal ions.

The main challenge in the synthesis of crystalline solid-state materials is altering the chemical composition without changing the underlying topology.<sup>6</sup> The tunable composition ratio of central metals is advantageous because controlling the banding gap becomes possible. Such tunability can lead to satisfactory electrochemical property. However, to the best of our knowledge, cation-exchanged single crystals have not been utilized to prepare

multi-metal nanomaterials. Currently, multi-metal sulfides are considered promising electrode materials that are specifically activated in supercapacitors<sup>7</sup> and lithium ion batteries;<sup>8</sup> these materials have catalytic properties,<sup>9</sup> Multi-metal sulfides have high redox activity and electrochemical activity and are inexpensive. However, multiple reactants, i.e., two or more inorganic salts or oxides that are present during preparation, may negatively affect the control of reaction rates and homogeneity. Such negative effects could contribute to the difficulty of large-scale preparation of materials with distinct morphology.

Our strategy for synthesis large scale regular 3D hierarchical  $\text{Ni}_x\text{Co}_{3-x}\text{S}_4$  ( $x = 0.15\text{--}0.42$ ) microflowers utilizes cobalt coordination complex and its ion exchanged derivatives as precursor because this method has given the high yield and the reaction conditions which are suitable for the small chemical factories. The as-synthesized  $\text{Ni}_x\text{Co}_{3-x}\text{S}_4$  microflowers showed high specific capacitance, excellent rate capacity, and good cycling stability, and such characteristics contribute to the potential of these microflowers as electrode materials for high performance supercapacitors. We investigated the process of central metal ion exchange to determine the tunable properties caused by cation-exchanged-induced SCSC transformation between the cobalt coordination complex and the cation-exchanged products. The perfectly designed electrodes showed higher electrochemical performance than the parent material. The results can help improve product properties as a response to energy crisis.

## Experimental Section

### Materials and methods

All the chemicals and solvents used were of analytic grade purity and used without further purification.

### The preparation of Nickel-exchanged compound

Single crystals of  $\{[\text{NaCo}_3(\text{TMA})_2(\mu_3\text{-OH})(\mu_2\text{-H}_2\text{O})_4(\text{H}_2\text{O})_7] \cdot 1.5\text{H}_2\text{O}\}_n$  (**1**) were prepared as described in the literature.<sup>25</sup> A series of nickel ion-exchanged crystals were obtained by immersing big crystals of the as-synthesized **1** into an ethanol solution with 40 mg/mL nickel nitrate for different replacement durations (1/3, 1, 2, 3, 5, 6, and 8 h) at 160 °C. Finally, the as-synthesized products were separated by filtration and washed sequentially with deionized water and 95% ethanol, and dried at room temperature.

### 10 Synthesis of 3D hierarchical $\text{Ni}_x\text{Co}_{3-x}\text{S}_4$ microflowers

In a typical preparation procedure, 1 mmol of nickel-exchanged compounds for 1h, 0.25 mL of glacial acetic acid, and 5mL of the ethylene glycol solvent were added to a 20 mL beaker under heating and stirring. Subsequently, 1 mmol of thiourea was dissolved in 11 mL ethanediamine to give a homogeneous solution, and then added drop wisely to the above mixture solution. After being stirred for 8 h, the mixed solution was transferred to a 20 mL Teflon-sealed autoclave, maintained at 160 °C for 24 h and cooled to room temperature naturally. After the solvothermal reaction,  $\text{Ni}_x\text{Co}_{3-x}\text{S}_4$  microflowers were formed.

To achieve controllable component,  $\text{Ni}_{0.24}\text{Co}_{2.76}\text{S}_4$ , and  $\text{Ni}_{0.42}\text{Co}_{2.58}\text{S}_4$  were synthesized using nickel-exchanged compounds for 3h and 6h respectively as precursors with a similar method to above. Finally, the black powder were washed several times with distilled water and 95% ethanol, and dried at 60 °C for 8 h in a vacuum oven.

### Characterization

X-ray diffraction (XRD) patterns were obtained with a Bruker D8 Advance X-ray powder diffractometer using Cu-K $\alpha$  irradiation at a scan rate of 0.1° s<sup>-1</sup>. XRD measurements of single crystal **1** and nickel-exchanged complex were performed within 5° ≤ 2θ ≤ 50°. XRD measurements of  $\text{Ni}_x\text{Co}_{3-x}\text{S}_4$  materials were performed within 10° ≤ 2θ ≤ 70°. Crystallographic data were collected on a Bruker SMART APEX CCD diffractometer using graphite-monochromatized Mo K $\alpha$  radiation (λ = 0.71073 Å) at room temperature. The morphologies and sizes of the as-prepared  $\text{Ni}_x\text{Co}_{3-x}\text{S}_4$  microflowers were characterized with a Zeiss EVO LS-15 scanning electron microscope (SEM) equipped with an energy-dispersive X-ray spectroscopy (EDS) system. The microstructures of the resulting  $\text{Ni}_{0.42}\text{Co}_{2.58}\text{S}_4$  materials were recorded with a JEOL JEM-2010 transmission electron microscope (TEM). The X-ray photoelectron spectroscopy (XPS) of the as-obtained  $\text{Ni}_{0.42}\text{Co}_{2.58}\text{S}_4$  microflower was collected using a Kratos AXIS ULTRA X-ray photoelectron microscope with Al-K $\alpha$  X-rays as the excitation source.

### Electrochemical performance test

Cyclic voltammetry (CV) measurements were carried out a CHI604E electrochemical workstation (Chenhua, Shanghai, china) at voltage scan rates range from 1 to 5000mV s<sup>-1</sup>. Electrochemical measurements were conducted in a three-electrode mode in 2 M KOH electrolyte. In this case, the 80% of the active material, 10% each of the carbon black and polyvinylidene difluoride (PVDF) were uniform mixed and then cast onto a nickel foam, which was used as a working electrode. A saturated Hg/HgO electrode and a platinum plate were employed as the reference and counter electrode, respectively. The galvanostatic charge-discharge tests were conducted with

current densities of 0.5, 1, 2, 5, 10, and 20 A/g using a LAND battery test system (CT2001A model). Specific capacitance could be calculated according to the following equation:  $C = I\Delta t/m\Delta V$ , where I is charge or discharge current, Δt is the time for a full charge or discharge, m indicates the mass of the active material, ΔV represents the practical voltage in a full discharge process. The cyclic stabilities were investigated using galvanostatic charge-discharge measurements at constant current densities of 2 A g<sup>-1</sup> for 1000 cycles.

## Results and discussion

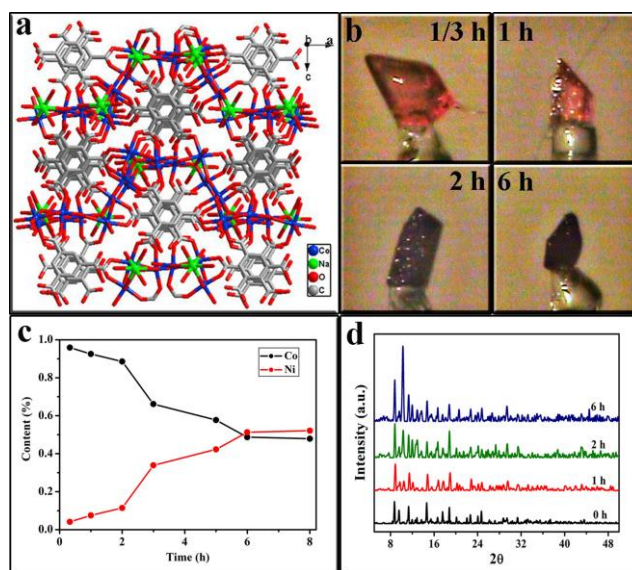


**Fig. 1** (a) Crystal packing of single crystal **1** (viewed on the b-a axis). (b) Images of Ni<sup>2+</sup>-exchanged single crystals after 1/3, 1, 2, and 6 h. (c) EDX spectra of Ni<sup>2+</sup>-exchanged single crystals for 1/3, 1, 2, 3, 5, 6, and 8 h. (d) XRD patterns of single crystals of **1**, and Ni<sup>2+</sup>-exchanged single crystals for 1, 2, and 6 h.

Single crystals of  $\{[\text{NaCo}_3(\text{TMA})_2(\mu_3\text{-OH})(\mu_2\text{-H}_2\text{O})_4(\text{H}_2\text{O})_7] \cdot 1.5\text{H}_2\text{O}\}_n$  (**1**) were obtained by the reaction of cobalt (II) sulfate with trimesic acid ( $\text{H}_3\text{TMA} = 1,3,5$ -benzenetricarboxylic acid) under pH 6.9; pH was adjusted using 0.5 M NaOH.<sup>10</sup> A series of nickel ion-exchanged crystals were obtained by immersing big crystals of the as-synthesized **1** into an ethanol solution with 40 mg/mL nickel nitrate for different replacement durations (1/3, 1, 2, 3, 5, 6, and 8 h) at 160 °C. Figs. 1a and 1b present the typical crystal packing images of the as-prepared single crystalline **1** and its nickel-exchanged products, respectively. Nickel-exchanged crystals entirely maintained the original shape of **1**. However, the color of nickel ion-exchanged crystals turned fuchsia (Fig. 1b), whereas such change was not observed in **1**. No further changes in color and in composition were observed after 6 h. Given that the rate of solvent and ligand exchanged depended on the nature of each cation, this duration suggests that the ion metathesis reactions reached equilibrium after 6 h. Infrared spectra and powder X-ray diffraction analysis revealed that single crystal **1** and Ni ion-exchanged crystals have similar absorbance and diffraction peaks, thereby indicating the presence of SCSC transformations induced by cation exchange and the creation of Ni-Co complexes. Ni-Co complexes were carefully analyzed by using energy dispersive X-ray spectroscopy.

The ratios of nickel to cobalt were 95.87:4.13, 92.50:7.50, 88.57:11.43, 66.11:33.89, 57.72:42.28, 48.72:51.28 and 47.90:52.10. (Fig. 1c) Analysis of single-crystal X-ray diffraction as shown in Fig. 1d revealed that nickel ion-exchanged crystals

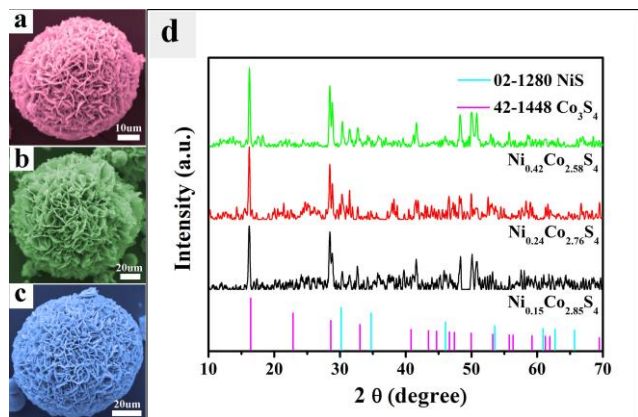


**Fig. 2** Scanning electron microscopy (SEM) images and X-ray diffraction (XRD) patterns of the as-synthesized  $\text{Ni}_x\text{Co}_{3-x}\text{S}_4$  ( $x = 0.15\text{--}0.42$ ): (a)  $\text{Ni}_{0.15}\text{Co}_{2.85}\text{S}_4$ , (b)  $\text{Ni}_{0.24}\text{Co}_{2.76}\text{S}_4$ , (c)  $\text{Ni}_{0.42}\text{Co}_{2.58}\text{S}_4$ , and (d)  $\text{Ni}_x\text{Co}_{3-x}\text{S}_4$  ( $x = 0.15\text{--}0.42$ ).

We prepared 3D hierarchical  $\text{Ni}_x\text{Co}_{3-x}\text{S}_4$  ( $x = 0.15\text{--}0.42$ ) microflowers using Ni–Co precursors with different Ni:Co atomic ratios of 92.50:7.50, 66.11:33.89, and 48.72:51.28 under ambient conditions. However, due to metal ion sorption and exchange could be achieved directly by suspending such coordination compounds in a solution containing metal salt.<sup>5</sup> The solution concentration of metal ions affects the ion sorption and

exchange behavior. When the solution concentration of metal salts is higher, metal ion sorption is mainly occurring, whereas metal ion exchange mainly takes place at a low solution concentration of metal salt. EDX and ICP could not give the amount of metal ions clearly but a macro quantity. Therefore, only a small range of Ni content in  $\text{Ni}_x\text{Co}_{3-x}\text{S}_4$  materials. The panoramic SEM image showed that the  $\text{Ni}_x\text{Co}_{3-x}\text{S}_4$  materials were highly uniform large-scale microflowers. The magnified SEM images (Figs. 2a, 2b, and 2c) revealed that each microflower was a hierarchical microsphere assembled by numerous bent nanosheets, which endow this structure with a high surface area, providing sufficient electrolyte-electrode interface for fast diffusion and reaction.<sup>10b, c</sup> The Ni/Co atomic ratios of  $\text{Ni}_{0.15}\text{Co}_{2.85}\text{S}_4$ ,  $\text{Ni}_{0.24}\text{Co}_{2.76}\text{S}_4$ , and  $\text{Ni}_{0.42}\text{Co}_{2.58}\text{S}_4$  were confirmed by energy-dispersive X-ray spectroscopy. The clear lattice fringes were visible from the high-resolution transmission electron microscopy image, and the distance (2.85 Å) between the adjacent lattice fringes corresponded to the (311) plane of  $\text{Co}_3\text{S}_4$  crystals (JCPDS no. 42–1448).  $\text{Ni}_{0.42}\text{Co}_{2.58}\text{S}_4$  microflower (220) and (311) crystal planes were clearly observed from the selected area electron diffraction image. The crystal nature is further confirmed by XRD data, as shown in Fig. 2d. Although  $\text{Ni}_x\text{Co}_{3-x}\text{S}_4$  microflowers have maintained most of the lattice fringe in  $\text{Co}_3\text{S}_4$  and part of lattice fringe of NiS. As a new type of materials, it is not consist of individual  $\text{Co}_3\text{S}_4$  and NiS. So there are some other peaks in XRD. X-ray photoelectron spectroscopy (XPS) times support our results. The Co 2p spectrum was fitted in such a way that two spin-orbit doublet characteristics of  $\text{Co}^{2+}$  and  $\text{Co}^{3+}$  and two shakeup satellites were present. The Ni 2p spectrum was also fitted in such a way that the spin-orbit doublet characteristic of  $\text{Ni}^{2+}$  was evident. Similarly, the S 2p emission spectrum was fitted with a spin-orbit doublet, which was a characteristic of  $\text{S}^{2-}$ .

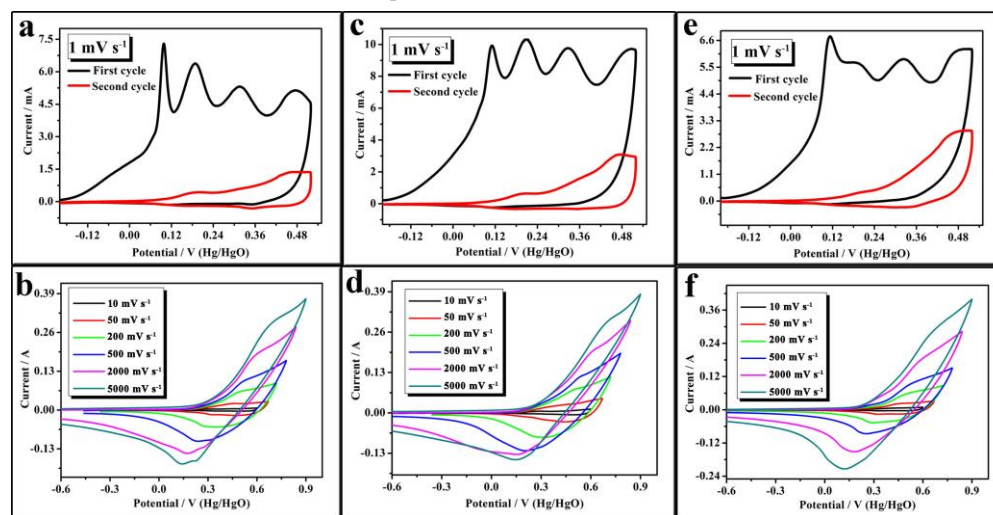


**Fig. 3** CV curves of the as-synthesized  $\text{Ni}_x\text{Co}_{3-x}\text{S}_4$  ( $x = 0.15\text{--}0.42$ ): (a to b)  $\text{Ni}_{0.15}\text{Co}_{2.85}\text{S}_4$ , (c to d)  $\text{Ni}_{0.24}\text{Co}_{2.76}\text{S}_4$ , and (e to f)  $\text{Ni}_{0.42}\text{Co}_{2.58}\text{S}_4$  at various scan rates.

To obtain information on the electrochemical properties of the as-synthesized  $\text{Ni}_x\text{Co}_{3-x}\text{S}_4$ , we characterized the electrodes by cyclic voltammetry (CV) and galvanostatic charge/discharge techniques. Figs. 3a, 3c, and 3e show the typical CV curves of  $\text{Ni}_{0.15}\text{Co}_{2.85}\text{S}_4$ ,  $\text{Ni}_{0.24}\text{Co}_{2.76}\text{S}_4$ , and  $\text{Ni}_{0.42}\text{Co}_{2.58}\text{S}_4$  electrodes at a scan rate of  $1\text{ mV s}^{-1}$ . The initial curve was different from those

in subsequent cycles, and such difference was due to the phase transformation from  $\text{Ni}_x\text{Co}_{3-x}\text{S}_4$  to  $\text{Ni}(\text{OH})_2$  (or  $\text{Co}(\text{OH})_2$ ) during the first positive sweep, as described in reaction (1).<sup>11</sup> Therefore, the phase transformation reaction occurred first and was followed by the oxidation reaction from  $\text{M}(\text{OH})_2$  to  $\text{MOOH}$  during the first positive sweep. Furthermore, only the reversible reduction

reaction from MOOH to M(OH)<sub>2</sub> (M=Ni and Co species) occurred during the first negative sweep. Only reversible redox reactions [reaction (2)] that occurred in subsequent CV cycle tests were observed. The XPS spectra of Ni<sub>0.42</sub>Co<sub>2.58</sub>S<sub>4</sub> show that the as-synthesized Ni<sub>0.42</sub>Co<sub>2.58</sub>S<sub>4</sub> contains three kinds of cations (Ni<sup>2+</sup>, Co<sup>2+</sup>, and Co<sup>3+</sup>). After the first positive sweep and at a scan rate of 0.5 mV s<sup>-1</sup>, most of the divalent cations in Ni<sub>0.42</sub>Co<sub>2.58</sub>S<sub>4</sub> are transformed into trivalent cations during the oxidation process. The absence of full oxidation in Ni<sub>0.42</sub>Co<sub>2.58</sub>S<sub>4</sub> may be due to the inappropriate scan rate. The reaction mechanism of Ni<sub>x</sub>Co<sub>3-x</sub>S<sub>4</sub> is given below.<sup>11, 12</sup>

The phase transformation reaction is as follows:



The reversible redox reaction is as follows:



Figs. 3b, 3d, and 3f show the typical CV curves of Ni<sub>0.15</sub>Co<sub>2.85</sub>S<sub>4</sub>, Ni<sub>0.24</sub>Co<sub>2.76</sub>S<sub>4</sub>, and Ni<sub>0.42</sub>Co<sub>2.58</sub>S<sub>4</sub> electrodes at scan rates of 10, 50, 200, 500, 2000, and 5000 mV s<sup>-1</sup>. The CV profiles showed the pronounced pseudocapacitive characteristics with a pair of reversible redox peaks within each voltammogram. The peak currents increased with increasing scan rate. Furthermore, the oxidation and reduction peaks of the Ni<sub>x</sub>Co<sub>3-x</sub>S<sub>4</sub> microflower electrode gradually shifted to the right and left with increasing scan rate, which is possibly due to the insufficient active material involved in the redox reaction under higher scan rates.<sup>12b</sup> Moreover, when the electrode has high sweep rates, massive OH<sup>-</sup> ions are required to intercalate swiftly at the interface of the electrode/electrolyte; however, relatively low concentration of OH<sup>-</sup> ions could not meet this demand and the processes would be controlled by the diffusion of ions. When the scan rate increased to 5000 mV s<sup>-1</sup>, the redox peaks of Ni<sub>0.15</sub>Co<sub>2.85</sub>S<sub>4</sub>, Ni<sub>0.24</sub>Co<sub>2.76</sub>S<sub>4</sub>, and Ni<sub>0.42</sub>Co<sub>2.58</sub>S<sub>4</sub> were still apparent, thereby indicating that Ni<sub>0.15</sub>Co<sub>2.85</sub>S<sub>4</sub>, Ni<sub>0.24</sub>Co<sub>2.76</sub>S<sub>4</sub>, and Ni<sub>0.42</sub>Co<sub>2.58</sub>S<sub>4</sub> have excellent rate performance.

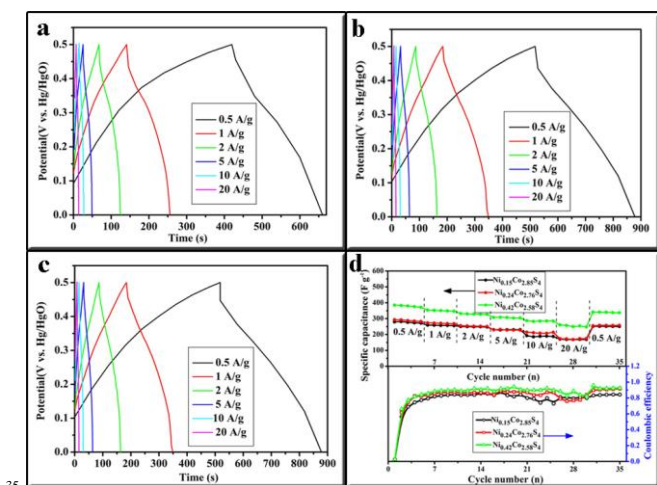


**Fig. 4** The galvanostatic charge–discharge curves of (a) Ni<sub>0.15</sub>Co<sub>2.85</sub>S<sub>4</sub>, (b) Ni<sub>0.24</sub>Co<sub>2.76</sub>S<sub>4</sub>, and (c) Ni<sub>0.42</sub>Co<sub>2.58</sub>S<sub>4</sub> at various current densities. (d) The discharge-specific capacitance and the coulombic efficiency curve of Ni<sub>0.15</sub>Co<sub>2.85</sub>S<sub>4</sub>, Ni<sub>0.24</sub>Co<sub>2.76</sub>S<sub>4</sub>, and Ni<sub>0.42</sub>Co<sub>2.58</sub>S<sub>4</sub> at different current densities.

To further evaluate the application potential of various Ni<sub>x</sub>Co<sub>3-x</sub>S<sub>4</sub> as electrodes for supercapacitors, galvanostatic charge–discharge measurements were performed between 0 and ~0.5 V (vs. Hg/HgO) at different current densities (Figs. 4a to 4c). The potential plateaus in the charge–discharge curves were consistent

with the results of the CV test, indicating the existence of Faradaic progress. The super capacitance and coulombic efficiency of all Ni<sub>x</sub>Co<sub>3-x</sub>S<sub>4</sub> electrodes could be calculated based on the charge–discharge curves. The results are plotted in Figure 4d. Ni<sub>0.42</sub>Co<sub>2.58</sub>S<sub>4</sub> microflowers exhibited higher average discharge capacitance values of 379.0, 350.4, 329.3, 306.2, 284.64, and 253.9 F g<sup>-1</sup> at various current densities of 0.5, 1, 2, 5, 10, and 20 A/g, respectively, than Ni<sub>0.24</sub>Co<sub>2.76</sub>S<sub>4</sub> (288.0 F g<sup>-1</sup> to 172.7 F g<sup>-1</sup> at 0.5 A/g to 20 A/g) and Ni<sub>0.15</sub>Co<sub>2.85</sub>S<sub>4</sub> (276.7 F g<sup>-1</sup> to 169.1 F g<sup>-1</sup> at 0.5 A/g to 20 A/g) (Fig. 4d). The increased electrochemical capacitance of the as-obtained Ni<sub>x</sub>Co<sub>3-x</sub>S<sub>4</sub> can be due to the presence of the nickel ions. Moreover, the Ni<sub>0.15</sub>Co<sub>2.85</sub>S<sub>4</sub>, Ni<sub>0.24</sub>Co<sub>2.76</sub>S<sub>4</sub>, and Ni<sub>0.42</sub>Co<sub>2.58</sub>S<sub>4</sub> have excellent rate performance with 67%, 60%, and 61% of the initial capacitance, respectively, when the charge–discharge rate was increased by 40 times from 0.5 A/g to 20 A/g. After continuous cycling for 30 cycles at the increased current densities of 0.5, 1, 2, 5, 10, and 20 A/g, the current density is reduced back to 0.5 A/g. The Ni<sub>0.15</sub>Co<sub>2.85</sub>S<sub>4</sub>, Ni<sub>0.24</sub>Co<sub>2.76</sub>S<sub>4</sub>, and Ni<sub>0.42</sub>Co<sub>2.58</sub>S<sub>4</sub> showed remarkable cycling stability, maintaining 90.8%, 89.3%, and 89.6% of the initial capacitance at 0.5 A/g. The supercapacitive performance of Ni<sub>x</sub>Co<sub>3-x</sub>S<sub>4</sub> microflowers was superior to that of commercial MnO<sub>2</sub>. The coulombic efficiency of Ni<sub>0.15</sub>Co<sub>2.85</sub>S<sub>4</sub>, Ni<sub>0.24</sub>Co<sub>2.76</sub>S<sub>4</sub>, and Ni<sub>0.42</sub>Co<sub>2.58</sub>S<sub>4</sub> was relatively high at approximately 95.8%, except in the first cycle because of the phase transformation reactions.

The cycling stability of Ni<sub>x</sub>Co<sub>3-x</sub>S<sub>4</sub> electrodes for 1000 cycles was tested by galvanostatic charge–discharge measurements at a current density of 2.0 A/g. As shown in Fig. 5a, the initial capacitance of Ni<sub>0.42</sub>Co<sub>2.58</sub>S<sub>4</sub> was approximately 321.4 F g<sup>-1</sup> and was subsequently decreased to 311.8 F g<sup>-1</sup>. Only 3% loss was observed after 1000 repeated cycles. Meanwhile, the initial capacitance of Ni<sub>0.24</sub>Co<sub>2.76</sub>S<sub>4</sub> was approximately 262.9 F g<sup>-1</sup>, which slightly decreased to 258.4 F g<sup>-1</sup> after 1,000 cycles, and the total capacitance loss was 2%. The specific capacitance of the Ni<sub>0.15</sub>Co<sub>2.85</sub>S<sub>4</sub> microflowers decreased from 222 F g<sup>-1</sup> to 214 F g<sup>-1</sup> with a capacitance retention of 96% after continuous processing for 1000 cycles. Moreover, the coulombic efficiency curves of Ni<sub>0.15</sub>Co<sub>2.85</sub>S<sub>4</sub>, Ni<sub>0.24</sub>Co<sub>2.76</sub>S<sub>4</sub>, and Ni<sub>0.42</sub>Co<sub>2.58</sub>S<sub>4</sub> (Fig. 5b) remain 95.03%, 97.0%, and 96.34%, respectively, after 1000 cycles at 2 A/g, which again demonstrated that Ni<sub>x</sub>Co<sub>3-x</sub>S<sub>4</sub> electrodes exhibit a higher degree of reversibility after a long-term cycling test.

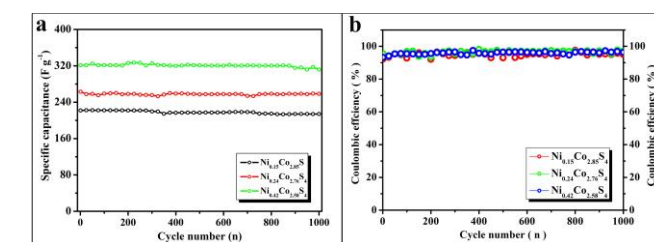


**Fig. 5** The cycling life (a) and coulombic efficiency curve (b) of Ni<sub>0.15</sub>Co<sub>2.85</sub>S<sub>4</sub>, Ni<sub>0.24</sub>Co<sub>2.76</sub>S<sub>4</sub>, and Ni<sub>0.42</sub>Co<sub>2.58</sub>S<sub>4</sub> at a current density of 2.0 A/g.

By contrast, the elevated levels of nickel ratio could benefit from capacitor performance of these materials. When nickel oxide alone is used as the electrode material, the performance of the supercapacitor was not satisfactory. The capacitance values of

$\text{Ni}_x\text{Co}_{3-x}\text{S}_4$  microflowers were higher than those of NiO nanowires ( $180 \text{ F g}^{-1}$  at  $0.5 \text{ A g}^{-1}$ ),<sup>13a</sup> NiO nanotubes ( $47 \text{ F g}^{-1}$  at  $0.28 \text{ A g}^{-1}$ ),<sup>13b</sup> and NiO with ordered mesoporous structure ( $120 \text{ F g}^{-1}$ ).<sup>13c</sup> Compared with  $\text{Ni}(\text{OH})_2$  and NiS materials with excellent performance, the capacitance performance of  $\text{Ni}_x\text{Co}_{3-x}\text{S}_4$  microflowers was slightly insufficient.  $\text{MnO}_2$  is the most commonly used supercapacitor electrode materials, the SC value for  $\text{Ni}_{0.42}\text{Co}_{2.58}\text{S}_4$  microflowers is  $379 \text{ F g}^{-1}$  at  $0.5 \text{ A/g}$ , which is more than ten times higher than the SC value of commercial  $\text{MnO}_2$  ( $\sim 36 \text{ F/g}$ ).<sup>14</sup> However, increasing the percentage content of central nickel ions can improve capacitive performance, which means that adjusting the metal center to the proper proportion is important. Thus, an ion-exchanged compound can be considered an appropriate precursor in the synthesis of multiple sulfide nanomaterials.

## Conclusions

In summary, Co–Ni complexes were successfully prepared by Ni exchange method. Cobalt coordination complex was used as precursor. SCSC transformation was achieved. We also synthesized large-scale regular 3D hierarchical  $\text{Ni}_x\text{Co}_{3-x}\text{S}_4$  ( $x = 0.15\text{--}0.42$ ) microflowers because of the different Co/Ni atomic ratios of Co–Ni complexes. The multi-metal sulfides prepared by this method showed better multi-metal ratios than those prepared by the co-precipitating method. The as-synthesized  $\text{Ni}_x\text{Co}_{3-x}\text{S}_4$  electrodes for supercapacitors exhibited excellent electrochemical performance and were tuned by adjusting the composition of products. The results of our study provide a novel electroactive material for designing next-generation supercapacitors. The conclusions section should come at the end of article.

## Acknowledgment

This work was supported by the National Science Foundation of China (Grant no. 21001090 and 21103153), and Program for Innovative Research Team (in Science and Technology) in University of Henan Province (Grant no. 2012IRTSTHN021) and Education Department of Henan Province (Grant no. 13A150648).

## Notes and references

<sup>a</sup> Center for Advanced Functional Materials Research, Zhongyuan University of Technology, Henan 450007, P. R. China; E-mail: [mlwz@163.com](mailto:mlwz@163.com)

<sup>b</sup> College of Chemistry and Molecular Engineering, Zhengzhou University, Henan 450001, P. R. China; E-mail: [chenweih@zzu.edu.cn](mailto:chenweih@zzu.edu.cn)

† Electronic Supplementary Information (ESI) available: [Figure S1–S4 (IR spectrums, SEM image, HRTEM image, SAED pattern, XPS spectra.) and the galvanostatic charge-discharge curve of the part of obtained samples]. See DOI: 10.1039/b000000x/

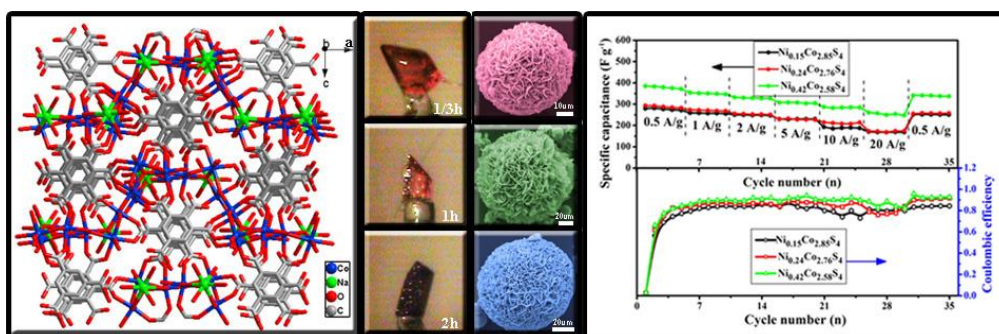
‡ Footnotes should appear here. These might include comments relevant to but not central to the matter under discussion, limited experimental and spectral data, and crystallographic data.

- 1 (a) S. E. Coe and R. S. Sussmann, *Diamond Relat. Mater.* 2000, **9**, 1726–1729; (b) E. C. Garnett and P. D. Yang, *J. Am. Chem. Soc.* 2008, **130**, 9224–9225; (c) B. Z. Tian, X. L. Zheng, T. J. Kempa, Y. Fang, N. F. Yu, G. H. Yu, J. L. Huang and C. M. Lieber, *Nature*, 2007, **449**, 885–888; (d) S. Kim, H. Y. Jeong, S. K. Kim, S. Y. Choi and K. J. Lee, *Nano Lett.* 2011, **11**, 5438–5442.
- 2 (a) J. A. Zhao, L. W. Mi, J. Y. Hu, H. W. Hou and Y. T. Fan, *J. Am. Chem. Soc.* 2008, **130**, 15222–15223; (b) H. Aggarwal, P. M. Bhatt,

- C. X. Bezuidenhout and L. J. Barbour, *J. Am. Chem. Soc.* 2014, **136**, 3776–3779; (c) T. F. Liu, L. F. Zou, D. W. Feng, Y. P. Chen, S. Fordham, X. Wang, Y. Y. Liu and H. C. Zhou, *J. Am. Chem. Soc.* 2014, **136**, 7813–7816.
- 3 (a) K. M. Hutchins, T. P. Rupasinghe, L. R. Ditzler, D. C. Swenson, J. R. G. Sander, J. Baltrusaitis, A. V. Tivanski and L. R. MacGillivray, *J. Am. Chem. Soc.* 2014, **136**, 6778–6781; (b) M. K. Sharma and P. K. Bharadwaj, *Inorg. Chem.* 2011, **50**, 1889–1897; (c) G. F. Liu, J. Liu, Y. Liu and X. T. Tao, *J. Am. Chem. Soc.* 2014, **136**, 590–593.
- 4 (a) R. Miyake and M. Shionoya, *Inorg. Chem.* 2014, **53**, 5717–5723; (b) B. F. Abrahams, A. D. Dharma, M. J. Grannas, T. A. Hudson, H. E. Maynard-Casely, G. R. Oliver, R. Robson and K. F. White, *Inorg. Chem.* 2014, **53**, 4956–4969; (c) X. N. Cheng, W. X. Zhang and X. M. Chen, *J. Am. Chem. Soc.* 2007, **129**, 15738–15739.
- 5 (a) L. W. Mi, H. W. Hou, Z. Y. Song, H. Y. Han, H. Xu, Y. T. Fan and S. W. Ng, *Cryst. Growth Des.* 2007, **7**, 2553–2561; (b) L. W. Mi, H. W. Hou, Z. Y. Song, H. Y. Han, H. Xu and Y. T. Fan, *Chem. Eur. J.* 2008, **14**, 1814–1821.
- 6 J. L. Atwood, L. J. Barbour, A. Jerga and B. L. Schottel, *Science*, 2002, **298**, 1000–1002.
- 7 (a) W. T. Wei, L. W. Mi, Y. Gao, Z. Zheng, W. H. Chen and X. X. Guan, *Chem. Mater.* 2014, **26**, 3418–3426; (b) L. Yu, L. Zhang, H. B. Wu and X. W. Lou, *Angew. Chem. Int. Ed.* 2014, **53**, 3711–3714.
- 8 (a) R. B. Wu, X. K. Qian, K. Zhou, J. Wei, J. Lou and P. M. Ajayan, *ACS Nano*, 2014. DOI: 10.1021/nn501783n; (b) X. H. Cao, B. Zheng, X. H. Rui, W. H. Shi, Q. Y. Yan and H. Zhang, *Angew. Chem. Int. Ed.* 2014, **53**, 1404–1409; (c) J. C. Bear, N. Hollingsworth, P. D. McNaughton, A. G. Mayes, M. B. Ward, T. Nann, G. Hogarth and I. P. Parkin, *Angew. Chem. Int. Ed.* 2014, **53**, 1598–1601.
- 9 (a) L. W. Mi, W. T. Wei, Z. Zheng, G. S. Zhu, H. W. Hou, W. H. Chen and X. X. Guan, *Nanoscale*, 2014, **6**, 1124–1133; (b) D. Merki, H. Vrubel, L. Rovelli, S. Fierro and X. Hu, *Chem. Sci.*, 2012, **3**, 2515–2525; (c) Y. H. Zhang, N. Zhang, Z. R. Tang and Y. J. Xu, *Chem. Sci.*, 2012, **3**, 2812–2822.
- 10 (a) D. P. Cheng, M. A. Khan and R. P. Houser, *Cryst. Growth Des.* 2004, **4**, 599–604. (b) C. Yuan, J. Li, L. Hou, X. Zhang, L. Shen and X. W. Lou, *Adv. Funct. Mater.* 2012, **22**, 4592–4597. (c) X. Y. Liu, Y. Q. Zhang, X. H. Xia, S. J. Shi, Y. Lu, X. L. Wang, C. D. Gu and J. P. Tu, *J. Power Sources*, 2013, **239**, 157–163.
- 11 J. Yang, X. Duan, Q. Qin and W. Zheng, *J. Mater. Chem. A*, 2013, **1**, 7880.
- 12 (a) Y. H. Xiao, S. J. Liu, F. Li, A. Q. Zhang, J. H. Zhao, S. M. Fang and D. Z. Jia, *Adv. Funct. Mater.* 2012, **22**, 4052–4059. (b) L. B. Kong, C. L. Mao, C. Liu, Y. C. Luo and L. Kang, *J. Solid State Electrochem.* 2013, **17**, 1463–1471.
- 13 (a) H. Pang, Q. Y. Lu, Y. Z. Zhang, Y. C. Li and F. Gao, *Nanoscale*, 2010, **2**, 920–922; (b) H. Pang, Q. Y. Lu, Y. C. Li and F. Gao, *Chem. Commun.* 2009, 7542–7544; (c) C. C. Yu, L. X. Zhang, J. L. Shi, J. J. Zhao, J. H. Gao and D. S. Yan, *Adv. Funct. Mater.* 2008, **18**, 1544–1554.
- 14 W. Y. Ko, L. J. Chen, Y. H. Chen, W. H. Chen, K. M. Lu, J. R. Yang, Y. C. Yen and K. J. Lin, *J. Phys. Chem. C*, 2013, **117**, 16290–16296.

5

## TOC



10